ESC European Society of Cardiology

Cardiovascular Research (2019) **115**, 1757–1765
doi:10.1093/cvr/cvz083

Arrhythmogenic propensity of the fibrotic substrate after atrial fibrillation ablation: a longitudinal study using magnetic resonance imaging-based atrial models

Rheeda L. Ali[1†], Joe B. Hakim[1†], Patrick M. Boyle[1,2,3], Sohail Zahid[2], Bhradeev Sivasambu[4], Joseph E. Marine[4], Hugh Calkins[4], Natalia A. Trayanova[1,2,5*‡], and David D. Spragg[4‡]

[1]Institute for Computational Medicine, Johns Hopkins University, 3400 N Charles Street, 208 Hackerman, Baltimore, MD 21218, USA; [2]Department of Biomedical Engineering, Johns Hopkins University, 3400 N Charles Street, 208 Hackerman, Baltimore, MD 21218, USA; [3]Department of Bioengineering, University of Washington, Seattle, WA, USA; [4]Division of Cardiology, Johns Hopkins University School of Medicine, Baltimore, MD, USA; and [5]Department of Medicine, Johns Hopkins University School of Medicine, USA

Received 6 November 2018; revised 31 January 2019; editorial decision 19 March 2019; accepted 8 April 2019; online publish-ahead-of-print 12 April 2019

Time for primary review: 25 days

Aims Inadequate modification of the atrial fibrotic substrate necessary to sustain re-entrant drivers (RDs) may explain atrial fibrillation (AF) recurrence following failed pulmonary vein isolation (PVI). Personalized computational models of the fibrotic atrial substrate derived from late gadolinium enhanced (LGE)-magnetic resonance imaging (MRI) can be used to non-invasively determine the presence of RDs. The objective of this study is to assess the changes of the arrhythmogenic propensity of the fibrotic substrate after PVI.

Methods and results Pre- and post-ablation individualized left atrial models were constructed from 12 AF patients who underwent pre- and post-PVI LGE-MRI, in six of whom PVI failed. Pre-ablation AF sustained by RDs was induced in 10 models. RDs in the post-ablation models were classified as either preserved or emergent. Pre-ablation models derived from patients for whom the procedure failed exhibited a higher number of RDs and larger areas defined as promoting RD formation when compared with atrial models from patients who had successful ablation, 2.6 ± 0.9 vs. 1.8 ± 0.2 and 18.9 ± 1.6% vs. 13.8 ± 1.5%, respectively. In cases of successful ablation, PVI eliminated completely the RDs sustaining AF. Preserved RDs unaffected by ablation were documented only in post-ablation models of patients who experienced recurrent AF (2/5 models); all of these models had also one or more emergent RDs at locations distinct from those of pre-ablation RDs. Emergent RDs occurred in regions that had the same characteristics of the fibrosis spatial distribution (entropy and density) as regions that harboured RDs in pre-ablation models.

Conclusion Recurrent AF after PVI in the fibrotic atria may be attributable to both preserved RDs that sustain AF pre- and post-ablation, and the emergence of new RDs following ablation. The same levels of fibrosis entropy and density underlie the pro-RD propensity in both pre- and post-ablation substrates.

Keywords Atrial fibrillation • Modelling • Cardiac MRI • Fibrosis • Drivers

* Corresponding author. Tel: +1 410 516 4375; fax: +1 410 516 5294, E-mail: ntrayanova@jhu.edu

† The first two authors contributed equally to this study.

‡ The last two authors contributed equally as senior authors to this study.

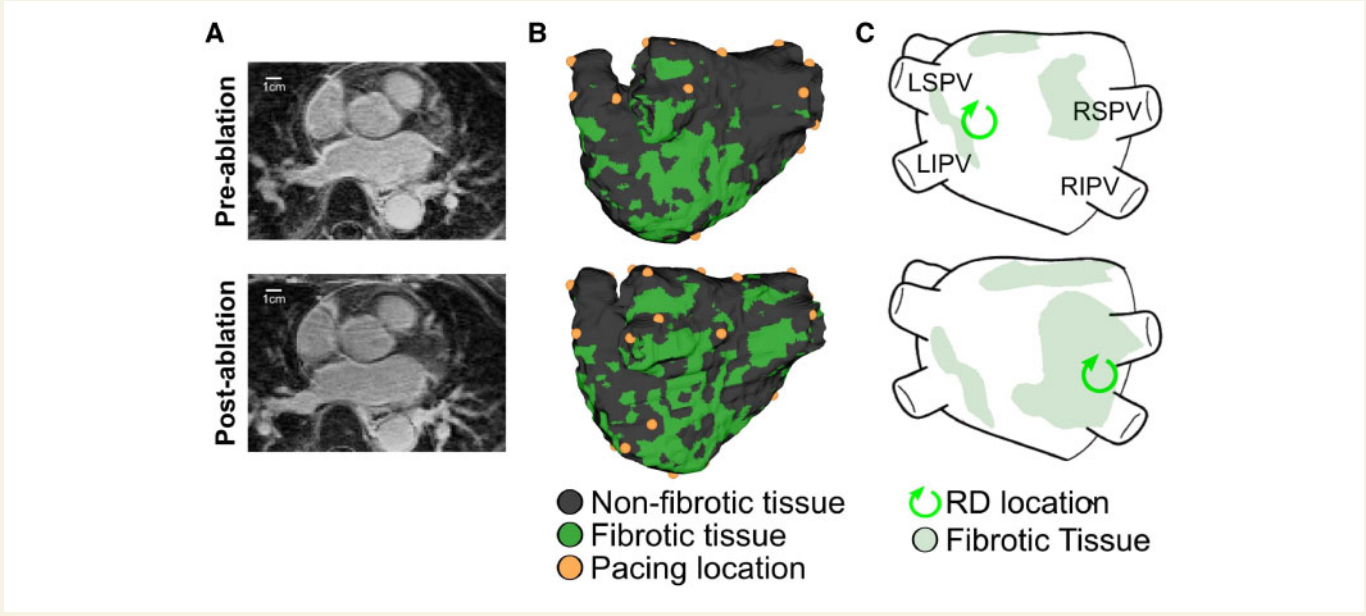

Figure 1 Overview of the study. Patient pre- and post-ablation cardiac LGE-MRI scans (*A*) were used to generate personalized pre- and post-ablation LA models incorporating the individual's atrial fibrosis distribution (*B*). The propensity of each model to sustain AF was assessed using rapid pacing from 30 uniformly distributed LA sites. The distribution of re-entrant drivers (RDs) sustaining AF in each pre-ablation model (*C*, top) was compared with that in the corresponding post-ablation model (*C*, bottom). (*C*) Represents schematically this comparison.

1. Introduction

Atrial fibrillation (AF) is the most common cardiac arrhythmia, and a major contributor to morbidity and mortality. Pulmonary vein (PV) isolation (PVI) is an established cornerstone of treatment for patients with either paroxysmal or persistent symptomatic AF.[1,2] However, in patients with significant atrial fibrosis, AF recurrence rates after PVI are high, resulting in freedom from AF of only 40–50% 1-year post-procedure.[3,4]

Research has suggested that proliferation of fibrosis in the atria can establish a substrate for AF initiation and perpetuation.[5,6] Regions of arrhythmogenic fibrosis may extend beyond the borders of traditional wide-area circumferential PVI, which could explain its relative ineffectiveness of PVI in patients with substantial atrial fibrosis. Cardiac late gadolinium enhancement (LGE)-magnetic resonance imaging (MRI) has been used to detect fibrosis in the atria based on the differences between signal intensities of remodelled tissue relative to those of normal myocardium.[3,7] Fibrosis, as identified on the pre-ablation LGE-MRI, has been used in clinical studies to guide catheter ablation of AF[3] and to predict the response to ablation.[8] LGE-MRI has also been acquired in clinical studies post-ablation, to investigate the link between ablation lesions, amount of residual fibrosis, and AF recurrence.[9]

Atrial LGE-MRI scans acquired pre-ablation have been used to construct patient-specific computational models of fibrotic atria.[10–17] Such models have revealed important insights regarding the fibrosis spatial distribution characteristics most conducive to AF perpetuation[13,17]; these insights have been corroborated by clinical evidence.[18] Personalized atrial models of the fibrotic substrate have been also used to predict AF ablation targets by identifying re-entrant drivers (RDs) sustaining AF. Computational predictions of AF ablation targets have been compared with those predicted by non-invasive electrocardiographic imaging[11] (ECGI) and by invasive focal impulse and rotor mapping[19] (FIRM), underscoring the utility of personalized atrial modelling.

In this study, we extend the application of atrial computational modelling to provide insight into the differences in AF propensity of atrial fibrotic substrates pre- and post-ablation. In a retrospective longitudinal study of 12 AF patients with pre- and post-ablation LGE-MRIs, we aim to evaluate the post-ablation changes in pro-fibrillatory mechanisms via simulations conducted in patient-specific models, and to establish whether failure of AF ablation resulted from inadequate termination of pre-ablation RDs or emergence of new RDs post-ablation.

2. Methods

2.1 Study population

This retrospective study included 12 AF patients, seven paroxysmal and five persistent, who received pre-procedural LGE-MRI scans between February 2014 and March 2016. Post-ablation MRIs were taken within 3–11 months after AF ablation. The investigation conformed to the principles outlined in the Declaration of Helsinki. Full patient characteristics are detailed in Supplementary material online, *Table S1*.

MRI acquisition was performed using a 1.5 T Avanto MR system. LGE-MRI scans were performed in the axial orientation 10–27 min following 0.2 mmol/kg of gadobenadimeglumine contrast agent using a fat-saturated 3-dimensional (3D) IR-prepared fast spoiled gradient recalled echo sequence, with electrocardiogram-triggered and respiratory navigator gating. Resolution was at 1.25 × 1.25 × 2.5 mm.

All patients had PVI either with radiofrequency (RF) or cryo-balloon ablation. Six patients underwent circumferential linear RF ablation around the left and right PVs. In three of the six RF ablation patients, a roof line had been created, connecting the circumferential lesions between the left and right superior PVs. The other six patients had cryo-ablation performed with either a 23 or 28 mm cryo-balloon (Arctic

Front and Arctic Front Advance, Medtronic Inc., Minneapolis, MN, USA). Patient follow-up was performed at 3 and 6 months.

Of the nearly 30 patients that have both pre- and post-ablation LGE-MRI scans, we chose 12 AF patients whose scans could be used for model construction. The rest of the scans had breathing artefacts, making them unusable for model construction.

2.2 Computational modelling

An overview of the simulation studies is presented in *Figure 1*. Pre- and post-ablation LGE-MRIs (*Figure 1A*) of the same patient were used to construct 3D pre- and post-ablation finite-element left atrial (LA) models, respectively (*Figure 1B*). Twenty-four 3D LA models were thus developed (12 model pairs). As in our previous publications,[11,13] LA regions were categorized as non-fibrotic or fibrotic myocardium based on the level of enhancement, resulting in a 3D reconstruction of the distribution of fibrosis in the left atrium. In both pre- and post-ablation models, the propensity of the fibrotic substrate to sustain AF was assessed by rapid pacing from 30 uniformly distributed LA locations (*Figure 1B*), as we have done previously.[11] This pacing protocol ensured that we capture all possible arrhythmias and enabled us to quantify the AF propensity of the patient-specific substrate. If AF was induced from a given pacing site, we determined the persistent RDs sustaining that AF episode; RDs have been previously shown to perpetuate AF in the fibrotic atria.[10,20] The distribution of induced RDs resulting from sequential pacing at all sites in each pre-ablation model (*Figure 1C*, top) was compared with that in the corresponding post-ablation model (*Figure 1C*, bottom) to determine the change in arrhythmogenesis in the fibrotic LA following ablation, in both patients with and without recurrent AF.

The geometric model reconstruction workflow is presented in recent publications.[13,17,21] In brief, the LA epicardial walls were manually segmented on the LGE-MRI using the software ITK-snap.[22] The right atria were excluded from this study as LGE-MRI quality there is low; furthermore, it has been previously shown that structural remodelling involves predominantly the left atrium.[23] The operator performing the segmentation was blinded as to whether the scan was pre- or post-ablation and to the clinical outcome of ablation. Using LA wall intensities and the mean blood pool intensity, fibrotic regions were identified as image voxels with Image Intensity Ratio (IIR) of more than 1.22.[13,24] Fibrosis burden was quantified for each model. High-resolution tetrahedral finite-element meshes were generated using an established approach.[25] Realistic fibre orientations were incorporated into each LA model using techniques and parameters described in our publications.[13,17]

Next, electrophysiological properties were assigned to non-fibrotic and fibrotic myocardium in the 24 geometric models as described previously;[17,21,26] these were the same in all models, as in our previous work with fibrotic atrial substrates. A human chronic AF atrial action potential model[27] with modifications to fit clinical monophasic action potential recordings from patients with AF[28] was used to represent membrane kinetics in non-fibrotic myocardium in all models. In the fibrotic regions of the atria, action potential modifications were additionally implemented, as done previously,[11,13,29,30] to represent the effect of elevated TGF-β1, a key component of the fibrogenic signalling pathway, by reducing maximal I_{K1}, I_{CaL}, and I_{Na} channel conductances.[13,17,27,28] Fibrotic regions were also assigned a 30% reduction in tissue conductivities.[31] This modelling strategy has shown good correlation to clinical results in retrospective patient studies.[11,13,17,19]

Propagation of electrical activity was simulated by solving the monodomain formulation coupled with the membrane model[32,33]; impulse conduction was anisotropic and depended upon local fibre orientation. The rapid pacing protocol for AF induction can be found in our previous publications.[13,17] Locations in the atria where RDs persisted were determined from RD phase singularity trajectories,[13] which were identified using the dynamic wavefront tip analysis method.[29] As these trajectories do not repeat exactly for every rotation cycle, they cover a region in each activation map. The activation maps were annotated by outlining the region that encompassed the RD trajectories during a 1000 ms-long analysis interval. The RD locations (i.e. the trajectory regions) in the post-ablation models were classified as either (i) unchanged from the pre-ablation model (preserved RDs) or (ii) unique to the post-ablation model (emergent RDs).

The remainder of model generation and the execution of simulations were automatic, except for the manually selected landmarks, which were used as an input for mapping the atlas' atrial fibres onto the atrial model.

2.3 Analysis of the fibrotic substrate from LGE-MRI

In our previous study,[13] we established that the spatial distribution of fibrosis, rather than total fibrosis burden, had important implications for promoting RD perpetuation. We found that areas of the fibrotic distribution that exhibited high fibrosis entropy (FE) and high fibrosis density (FD) were associated with high likelihood of RD localization. Areas with such fibrosis characteristics were typically boundary zones between fibrotic and non-fibrotic tissue; these findings were confirmed by ECGI clinical studies.[13,18]

Here, we used the same quantitative analysis as in our previous study,[13] constructing maps of FD and FE in all pre- and post-ablation LA models. In these maps, the local FD value indicates the proportion of fibrotic elements among all elements surrounding the given location, while the local FE value quantifies the level of disorganization between fibrotic and non-fibrotic elements in the local neighbourhood. Three-dimensional maps of calculated FD and FE values were then used to subdivide each patient-specific LA model into regions that have high likelihood of sustaining RDs (termed here pro-RD regions) and those that have low likelihood, as done previously.[13] To demarcate pro-RD regions, we used the classification scheme based on machine learning devised and then validated with clinical data in our previous study.[13] The classification polynomial used here, $0.4096FD^2 + 3.28(FD)(FE) - 0.1036\ FE^2 - 0.7112(FD) - FE + 0.0429$, was determined in that study.

3. Results

3.1 Pre-ablation LA fibrosis burden in patients with successful and failed AF ablation

During the follow-up period, 6 of the 12 patients were free from AF, and 6 had AF recurrence.

Figure 2A presents a comparison of the pre-ablation fibrosis burden (calculated as the number of finite elements as a percent of the total number of finite elements in each atrial model) in patients who had successful and in those that had failed PVI. The fibrosis burden was lower in

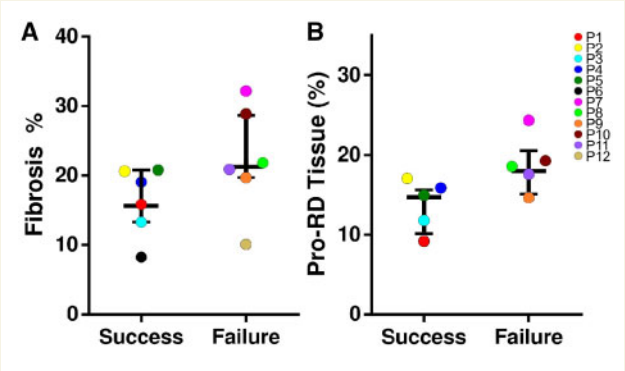

Figure 2 Characterization of the pre-ablation atrial substrate. (*A*) Percentage of pre-ablation fibrotic burden in LA models of patients with successful and failed ablation. (*B*) Percentage of pro-RD tissue (out of total LV volume) in pre-ablation models of patients with successful and failed ablation. Colours represent individual patients. Data are expressed as median and interquartile range.

patients with successful ablation than those with failed, 17.4 (13.2–20.6)% and 21.3 (19.7–28.9)% [median (interquartile range)], respectively. This relation between fibrosis burden and clinical outcome demonstrates that our cohort is consistent with previous clinical observations.[23]

3.2 Pro-arrhythmic propensity of LA fibrotic substrate pre- and post-ablation

In 10 of the 12 pre-ablation LA models, AF sustained by RDs (AF-RD) was induced. In another pre-ablation model, AF was sustained by a macro-reentrant circuit around the left inferior PV; fibrosis burden in this model was low, 8.94%. In the remaining LA model, AF could not be induced. In this model, atrial fibrosis burden was very low, 7.39%, indicating that mechanisms other than fibrosis could have potentially sustained AF in this patient.

For the 10 AF-RD cases, *Figure 2B* compares the extent of tissue classified as pro-RD (based on FD and FE quantification from LGE-MRI, as described in Section 2) in pre-ablation LA models from patients who had successful vs. those who had failed ablation. The volume of pro-RD tissue was lower in patients with successful that those with failed procedure, 14.9 (10.5–16.4)% vs. 18.6 (16.1–21.8) % [median (interquartile range)].

3.3 Pre-ablation RDs are fully eliminated in LA models of patients with successful ablation

For the five AF-RD patients with successful PVI, a total of nine RDs were identified in the corresponding pre-ablation models: four were located on the inferior LA, three near the left PVs, and one adjacent to the right inferior PV. Importantly, in all five patients, none of these RDs were preserved in post-ablation models, as ablation completely eliminated them. *Table 1* presents detail regarding the RDs and their locations in the five AF-RD pre-ablation models from patients with successful ablation. Supplementary material online, *Figure S1* presents the locations of all RDs in these pre-ablation models.

Table 1 RDs in pre-ablation atrial models of patients with successful procedures

Patient ID	Number of RDs	RD locations	Number of pacing sites
P1	2	PLA, LIPV	4
P2	1	LIPV	2
P3	2	Right PLA, Left PLA	3
P4	2	Inf. LA, RIPV	4
P5	2	Inf. LA, LPV carina	5

Listed are number of RDs, total number of pacing sites that induced RDs in a given model, and RD locations.
Inf., inferior; LIPV, left inferior PV; PLA, posterior LA; RIPV, right inferior PV.

3.4 RDs in LA models of patients with failed ablation

Pre-ablation models derived from LAs of patients for whom the procedure later failed exhibited a higher number of RDs sustaining AF, when compared with those of patients who had successful ablation, 2 (1.5–2) vs. 2 (2–4) [median (interquartile range)]. Additionally, the number of pacing sites from which the RDs were induced in each of the pre-ablation LA models from patients with failed ablation was larger than that from patients with successful ablation 8 (3–14) vs. 4 (2.5–4.5) [median (interquartile range)], underscoring the higher pro-arrhythmic propensity of the fibrotic substrate in the former cases.

For the five AF-RD patients with failed ablation, a total of 13 RDs were identified in pre-ablation models. These RDs were located in the vicinity of the inferior posterior LA (5), anterior LA (1), left atrial appendage (LAA, 4), left PVs (2), and the right PVs (1). Detail regarding these RDs and their locations is presented in *Table 2*.

3.5 Preservation of RDs in LA models of patients with failed ablation

In contrast to models from patients with successful ablation, preserved RDs were seen in models from patients with failed ablation. In two of the five patients with recurrent AF after PVI, RDs were at identical atrial locations on pre- and post-ablation models (*Figure 3*), specifically, at the mid-posterior in one pair of models (*Figure 3A*), while the other model pair exhibited two preserved RDs, on the right and left inferior PVs (*Figure 3B*). This indicates that the inability of PVI to eliminate existing RDs is a potential mechanism for ablation failure.

To better illustrate the failure of ablation (via PVI or PVI plus roof line) by preserving RDs, we used the pre-ablation models of the five failed ablation patients and incorporated the corresponding ablation lesions (PVI or PVI plus roof line) followed by AF induction (*Figure 4*). To model the ablation lesions in each failed ablation patient, we used the corresponding CARTO maps, and mapped the tips of catheter during each ablation onto the model geometry (*Figure 4A*). The actual lesions were modelled as non-conductive spheres of radius 3.5 mm around the catheter tip points; the lesions were then made transmural and any gaps were filled. We compared the induced RDs in the *in silico* ablated models to those found in the corresponding pre-ablation models. Preservation of RD locations was observed in all five of the *in silico* ablated models (*Figure 4B*; four patient models are shown), despite the presence of PVI and roof line lesions.

Table 2 Number of RDs and pro-RD% in pre- and post-ablation atrial models of patients with recurrent AF

	Number of RDs		RD locations		Number of pacing sites	
Patient ID	Pre-ablation RDs	Post-ablation RDs (preserved RDs)	Pre-ablation	Post-ablation	Pre-ablation	Post-ablation
P7	2	1	ALA, inf. PLA	ALA	11	9
P8	2	1	ALA, LAA	PLA	4	4
P9	1	2 (1)	PLA	PLA, Roof	2	8
P10	2	5 (2)	PLA near RIPV, PLA near LIPV	PLA near RIPV PLA near LIPV ALA near LSPV, LAA LPV Carina	8	10
P11	6	2	LAA, PLA, Inf. PLA, PLA near LIPV, LPV carina, Inf. to the LAA	ALA near LSPV PLA near LSPV	17	2

The table lists number of RDs, indicating whether they are preserved RDs (number in parentheses); RD locations; the total number of pacing sites that induced RDs in a given model.
ALA, LA anterior wall; Ant., anterior; Inf., inferior; LIPV, left inferior PV; LPV, left PVs; LSPV, left superior PV; PLA, LA posterior wall; Pos., posterior; RIPV, right inferior PV.

3.6 Emergent RDs in post-ablation LA models

While there were preserved RDs in two of the five LA models from patients with failed ablation, as described above, emergent RDs were documented in all five post-ablation models derived from patients who had failed ablation (*Table 2*). These results indicate that PVI lesions create, in combination with unaffected fibrosis, a pro-arrhythmic substrate that gives rise to new RDs. These emergent RDs sustain recurrent AF, sometimes in combination with remaining RDs unaffected by ablation.

Emergent RDs were also inducible from a large number of pacing sites (*Table 2*), underscoring the high AF propensity of the post-ablation substrate. The maximum number of emergent RDs in a model was three; the results from that model are presented in *Figure 5*, where the three emergent RDs are at locations distinct from those in the corresponding pre-ablation model (emergent RD locations: anterior to LAA, inferior to LAA, and between the ostia of left veins). All emergent RDs in the remaining models were also at locations different from those in pre-ablation substrates (*Table 2*).

Finally, *Figure 6* presents another important novel insight: the emergent RDs phase singularity regions co-localized with pro-RD regions (regions determined by the algorithm described in Section 2, as those of high propensity for maintaining RDs). Of the eight emergent RDs in failed ablation models, 90.3 ± 9.0% of the elements contained within the corresponding RD trajectory regions were also classified as pro-RD. *Figure 6* illustrates this in two post-ablation LA models. Thus, not only the RDs in pre-ablation substrates (as found in our previous study[13]) but also the ones that emerge post-ablation (as found here) perpetuate only in regions with specific characteristics of fibrosis spatial distribution, those of high FD and FE. We found that in LA models from patients with failed PVI, the extent of pro-RD tissue post-ablation, 15.9 (15.6–25.2)%, was fairly similar to than pre-ablation, 18.5 (16.1–21.81)% [median (interquartile range)].

RDs in pre- and post-ablation models of patients with failed ablation not shown in the figures above are presented in Supplementary material online, *Figure S2*. Supplementary material online, *Videos S1* and *S2* of illustrative examples of AF in two models are also included.

4. Discussion

This retrospective study used personalized 3D atrial computational modelling to understand the change in AF propensity following ablation (PVI or PVI plus roof lines). To construct the models, we used LGE-MRIs of 12 patients for whom both pre- and post-ablation scans were acquired; in 10 of them AF sustained by RDs was inducible. LGE-MRI allowed us to represent in the models not only the individual atria shape, but also the patient-specific distribution of atrial fibrosis, as fibrosis architecture is highly variable from patient to patient, as well as from region to region within the atria of a given patient.[3,34] Comparison of RD dynamics in the fibrotic substrate prior to and after ablation in each patient revealed why AF recurred in some cases. Specifically, we found that AF success of PVI (or PVI plus roof lines) correlated with elimination of existing RDs and the absence of emergent RDs in the MRI-based LA models. Furthermore, AF recurrence correlated with the presence, in some post-ablation models, of RDs unaffected by ablation, and with the emergence of new RDs in all models, where these emergent RDs occurred at locations distinctly different from those of the original RDs.

Atrial fibrosis is a significant contributor to AF pathophysiology, as demonstrated by clinical and experimental research.[5,35] Fibrotic remodelling results in conduction heterogeneity and propagation block, and in the establishment of pro-fibrillatory substrate.[5,6] AF patients exhibit an increased expression of fibrosis components[36] and advanced interstitial fibrosis.[37] Furthermore, in AF patients with extensive (≥30%) LA fibrosis, AF ablation is more likely to fail.[8] Our results are consistent with these findings. Furthermore, the multicentre DECAAF study demonstrated that atrial fibrosis, estimated by LGE-MRI, was associated with an increased likelihood of AF recurrence following ablation.[3] Recent studies have also attempted to isolate the fibrotic regions[38] as part of an AF ablation strategy.

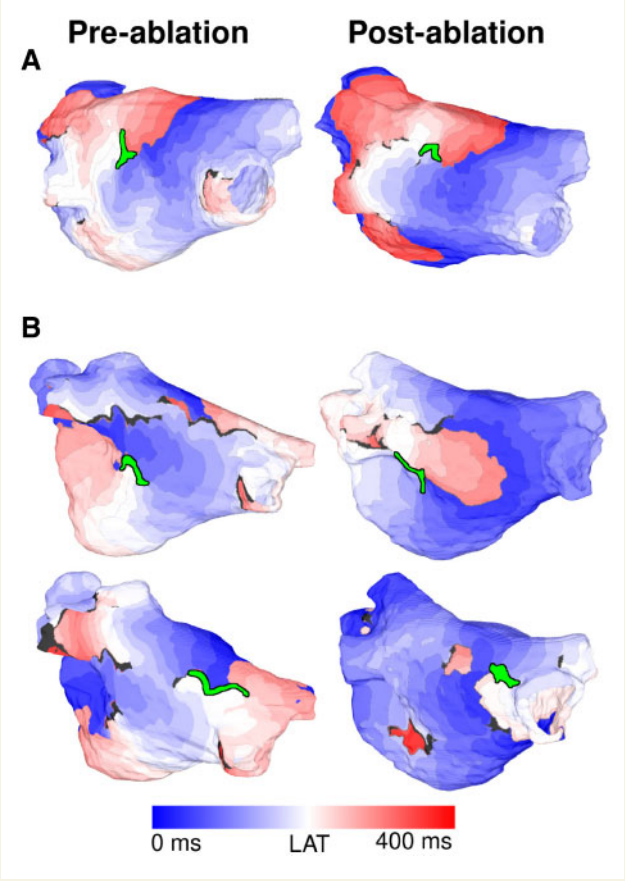

Figure 3 Preservation of RDs in models of patients with failed ablation. (*A* and *B*) Illustration of RD preservation in post-ablation models of two patients with failed ablation. AF activation maps are overlaid with RD phase singularity regions (green) to highlight the preserved RD locations. In *A*, there is one preserved RD on the mid posterior wall, while in *B*, there are two preserved RDs, on the left and right inferior ostium. LAT, local activation time.

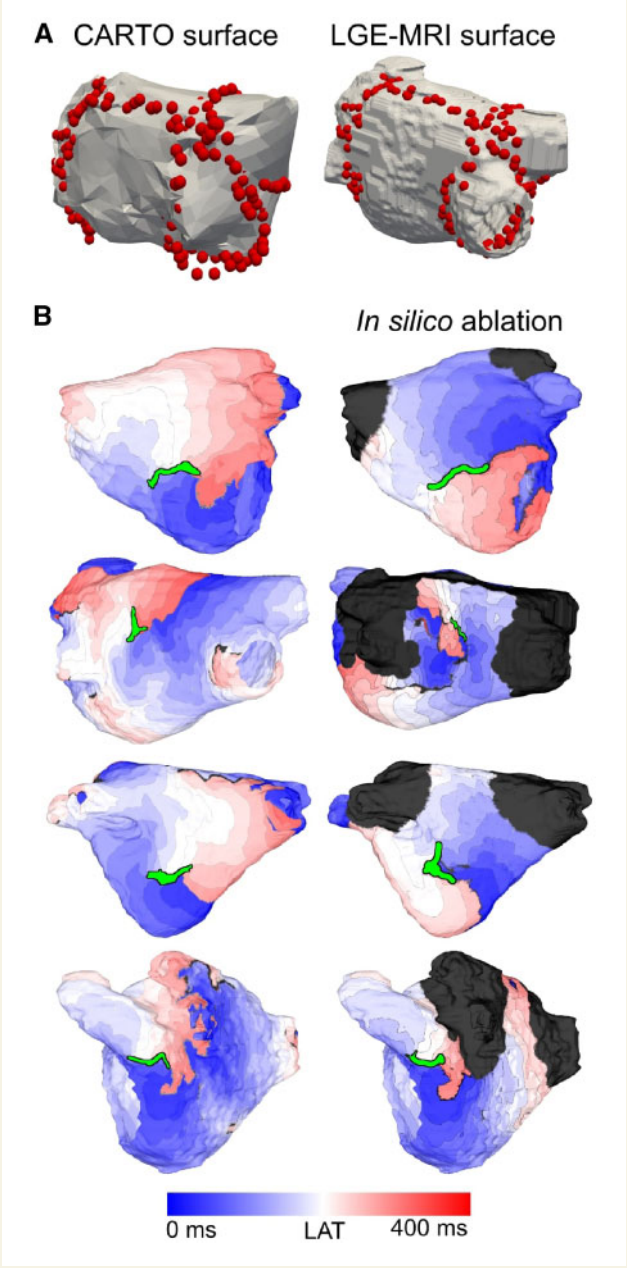

Figure 4 *In silico* ablation in models constructed from pre-ablation scans of patients with failed ablation. (*A*) Export of catheter ablation points (red) from the CARTO LA electro-anatomical surface, left, and their co-registration with the MRI model LA surface. For the patient shown in this illustration, ablation included PVI plus a linear ablation across LA roof. (*B*) Examples of *in silico* ablation in four pre-ablation models of patients who had failed clinical ablation. AF activation maps overlaid with RD phase singularity regions (green) are shown before (*B*, left) and after (*B*, right) *in silico* ablation. Dark grey indicates tissue which did not activate because of complete electrical isolation of the PVs following *in silico* ablation. LAT, local activation time.

Rotational electrical activity (rotors or RDs) have been shown to underlie human AF (see reviews[39,40]) Atrial fibrotic remodelling promotes the initiation and perpetuation of re-entrant activity, as evidenced by experimental[17,41–44] and clinical studies.[18] Dual-sided optical mapping of explanted human hearts has revealed that RDs are anchored to fibrosis-insulated atrial bundles.[43] Similar observations were made in sheep atria, where re-entrant circuits anchored to large fibrous patches on the posterior LA.[42] Furthermore, patient-specific computational models of the fibrotic atria of patients with persistent AF highlighted the role of fibrosis in RD dynamic localization in the remodelled substrate, demonstrating that fibrosis border zones with specific characteristics (those with high FD and high FE) are most likely to sustain RDs[13,45]; these findings have been corroborated by clinical evidence.[18]

Such computational modelling also revealed that not all potential RDs are manifested during a given clinical AF episode, and that there are additional locations in the fibrotic substrate prone to sustaining RDs.[13,17] Thus, recurrent AF could be due to RDs that arise at these latent locations. Accordingly, using longitudinal LGE-MRIs, the present study sheds light on the arrhythmogenic propensity of the fibrotic substrate pre- and post-ablation in patients with successful and failed ablation. Results demonstrate that in patients with recurrent AF, the fibrotic substrate prior to ablation has the capacity to harbour a higher number of RDs, potentially elevating the probability of ablation failure. Furthermore, the number of pacing sites from which the RDs were induced in each of the

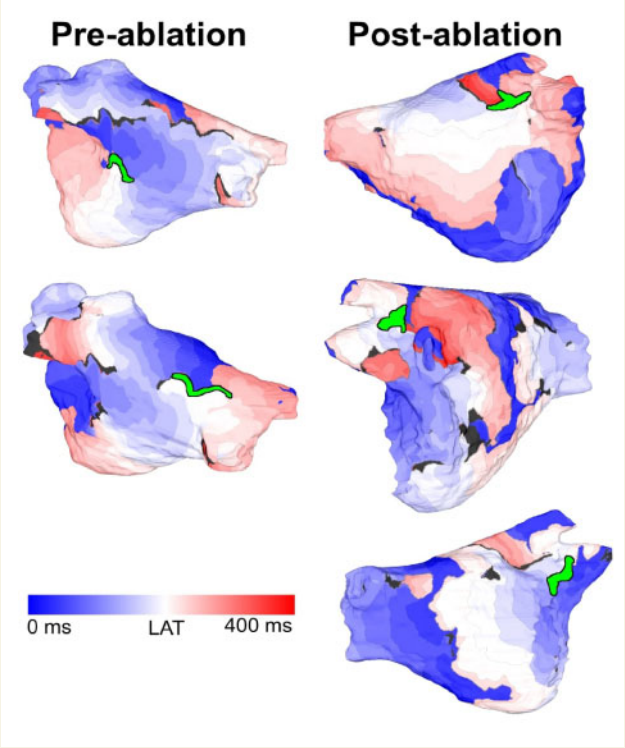

Figure 5 Emergent RDs in post-ablation models of patients with failed ablation. An example of emergent RDs in a patient with failed ablation (P10). RD trajectories (2) are shown in the pre-ablation (left) and in the post-ablation model (right, three distinct emergent RDs). Ablation failure in this patient is due to the emergence of new post-ablation RDs. LAT, local activation time.

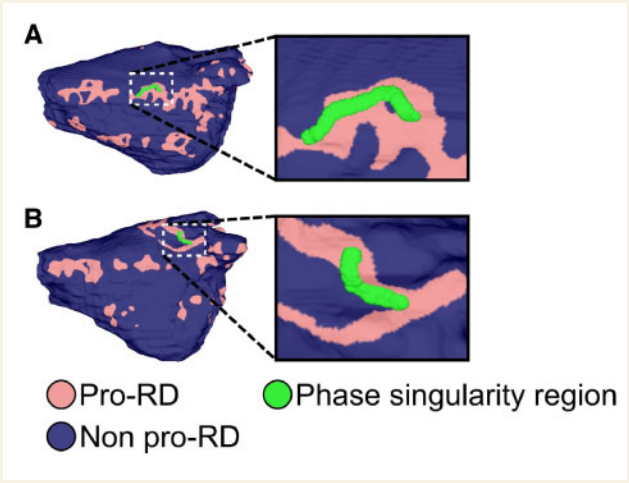

Figure 6 Spatial correlation of pro-RD regions with emergent RDs in post-ablation models of patients with failed ablation. Examples of emergent RD phase singularity regions in two post-ablation models (*A* and *B*) shown overlaid with Pro-RD atrial regions to highlight that emergent RD phase singularity regions exist predominantly in Pro-RD regions.

pre-ablation models of patients with recurrent AF is typically larger than those of patients with successful procedure, unmasking a more 'irritable' substrate.

In cases of successful ablation, PVI or PVI plus roof lines completely eliminated the RDs sustaining AF, likely because RD locations overlapped with the lesions. In patients for whom AF recurred, RDs were sometimes unaffected by PVI (or PVI plus roof lines), and in all cases new RDs emerged at different locations. These results have important implications for PVI, the current standard-of-care and is corroborated with evidence from FIRM studies,[46] where *de novo* RDs were documented in recurrent AF.

Our retrospective study analysed the characteristics of the spatial distribution of fibrosis in the pre- and post-ablation substrates from LGE-MRI scans. The analysis implemented here is based on our previous study,[13] which demonstrated that RDs perpetuate at regions, typically at the border between fibrotic and non-fibrotic areas, characterized with high FD and FE (areas of intermingling of non-fibrotic and fibrotic tissue, i.e. fibrosis disorganization). RDs were absent from both non-fibrotic sites or low-density (speckled) fibrotic tissue, and from regions of deep fibrosis (i.e. locations with high FD but low FE). The total fibrosis burden is implicitly accounted for in this pro-RD region analysis, the latter regions shown to have a direct mechanistic link to RD perpetuation. In our previous study,[13] we used machine learning to derive a general classification scheme separating the atria into pro-RD and non-pro-RD regions; the classification was then validated with ECGI clinical data.[13,18]

We used the same approach here to demarcate pro-RD regions, and found that the total volume of pro-RD regions in pre-ablation models was smaller in patients with successful ablation that those with failed ablation, indicating a pre-disposition to RD formation in the latter models. Furthermore, we found that in all cases of emergent RDs in post-ablation models, RD trajectories were contained predominantly in pro-RD regions, suggesting that the presence of pro-RD characteristics of the fibrotic substrate is a universal finding, and applies not only to pre-ablation substrates, but also to fibrotic substrates modified by failed ablation lesions. The presence of pro-RD tissue in post-ablation models helps explain why PVI fails, moreover that the amount of pro-RD tissue in post-ablation models of patients with failed PVI was higher than that pre-ablation.

The longitudinal cohort used in our study is heterogeneous, as it includes patients with paroxysmal and persistent AF pre-ablation, as well as with PVI and PVI plus roof lines. However, a unifying feature of all patients is that they have atrial LGE, i.e. fibrotic remodelling detectable on LGE-MRI, which constitutes the arrhythmogenic atrial substrate. As we analyse the presence of RDs in this fibrotic substrate and the distribution of pro-RD regions pre-ablation, cohort heterogeneity does not affect, mechanistically, the assessment of the arrhythmogenic propensity of the pre-ablation atrial substrate. Differences in amount of fibrosis between patients are also accounted for, inherently, in the pro-RD tissue analysis. Post-ablation, the resulting fibrotic substrate is analysed in the same way, regardless of how PVIs are isolated or whether roof lines were also executed. On LGE-MRI, one cannot distinguish between native fibrosis and fibrosis/scar caused by ablation.[47] Thus, overall, despite the heterogeneous cohort, we have the same mechanistic underpinning and the same analysis of the fibrotic substrate propensity to AF. Ablation generates a lesion distribution which combines with the residual native fibrosis distribution to give rise to a new post-ablation fibrosis distribution, which may or may not be arrhythmogenic (AF recurrence vs. successful ablation). Thus, successful ablation lesions turn a 'bad' fibrosis

distribution (one characterized with high entropy and density) into a 'good' fibrosis distribution (characterized with low entropy). In successful ablation, PVI lesions (plus roof lines sometimes) combine synergistically with residual native fibrosis, in such a way that the substrate is much less likely to give rise to RDs—the entropy (heterogeneity) of the resulting scar/fibrosis becomes low and the substrate no longer promotes RD formation and sustenance.

Finally, this study presents the largest number of patient-specific atrial models to date, 24 generated, of which 20 were utilized in rapid pacing simulations and RD analysis. It represents a significant computational undertaking and is one of the first forays into applying personalized computational modelling to address clinically relevant questions.

4.1 Clinical implications

The fact that RDs may be harboured in the fibrotic substrate at locations outside of standard PVI lesion set has clear clinical implications. Failure of PVI to successfully eliminate recurrent AF may be due to inadequate isolation of PV triggers. A different mechanism for recurrent AF after PVI is the presence of an arrhythmogenic substrate either not completely eliminated by PVI, or generated by catheter ablation itself, as suggested here. In the current investigation, we demonstrate that PVI failure is associated with both failure to eliminate pre-ablation RDs and emergence of new RDs following ablation. These observations suggest that personalization of ablation to target potentially pro-arrhythmic regions in the fibrotic substrate is worthy of broader investigation.

4.2 Limitations

As this study is longitudinal retrospective, with a heterogeneous cohort, its findings will need to be validated in a more homogenous prospective cohort of sufficient size. Prospective studies should be conducted to fully evaluate how ablation alters the fibrotic substrate and its propensity to AF. Additional limitation is that in post-ablation scans, no distinction can be made between native fibrosis and ablated tissue. Finally, only the LAs of patients were modelled here, as the quality of the LGE-MRI quality of the RA was lower. While most RDs have been reported in the left atrium,[48] research has also indicated that RAs could harbour as much as 30% of the total RDs and thus play a role in sustaining AF in patients with persistent form of the arrhythmia.[39] Bi-atrial models might need to be constructed to validate the mechanistic findings in this study.

Supplementary material

Supplementary material is available at *Cardiovascular Research* online.

Conflict of interest: none declared.

Funding

This work was supported by the National Institutes of Health [DP1-HL123271, U01-HL141074 to N.A.T.]; Leducq [16CVD02 to N.A.T.]; American Heart Association [16-SDG-30440006 to P.M.B.], a fellowship from Johns Hopkins University to R.L.A., the Edward St. John Fund for AF Research, the Roz and Marvin H Weiner and Family Foundation, the Dr Francis P. Chiaramonte Foundation, the Marilyn and Christian Poindexter Arrhythmia Research Fund, the Norbert and Louise Grunwald Cardiac Arrhythmia Research Fund and the Mr and Mrs Larry Small AF Research Fund.

References

1. Calkins H, Hindricks G, Cappato R, Kim Y-H, Saad EB, Aguinaga L, Akar JG, Badhwar V, Brugada J, Camm J, Chen PS, Chen SA, Chung MK, Nielsen JC, Curtis AB, Davies DW, Day JD, d'Avila A, de Groot NMSN, Di Biase L, Duytschaever M, Edgerton JR, Ellenbogen KA, Ellinor PT, Ernst S, Fenelon G, Gerstenfeld EP, Haines DE, Haissaguerre M, Helm RH, Hylek E, Jackman WM, Jalife J, Kalman JM, Kautzner J, Kottkamp H, Kuck KH, Kumagai K, Lee R, Lewalter T, Lindsay BD, Macle L, Mansour M, Marchlinski FE, Michaud GF, Nakagawa H, Natale A, Nattel S, Okumura K, Packer D, Pokushalov E, Reynolds MR, Sanders P, Scanavacca M, Schilling R, Tondo C, Tsao HM, Verma A, Wilber DJ, Yamane T. 2017 HRS/EHRA/ECAS/APHRS/SOLAECE expert consensus statement on catheter and surgical ablation of atrial fibrillation. *Heart Rhythm* 2017;**14**:e275–e444.
2. Pappone C, Rosanio S, Oreto G, Tocchi M, Gugliotta F, Vicedomini G, Salvati A, Dicandia C, Mazzone P, Santinelli V, Gulletta S, Chierchia S. Circumferential radiofrequency ablation of pulmonary vein ostia: a new anatomic approach for curing atrial fibrillation. *Circulation* 2000;**102**:2619–2628.
3. Marrouche NF, Wilber D, Hindricks G, Jais P, Akoum N, Marchlinski F, Kholmovski E, Burgon N, Hu N, Mont L, Deneke T, Duytschaever M, Neumann T, Mansour M, Mahnkopf C, Herweg B, Daoud E, Wissner E, Bansmann P, Brachmann J. Association of atrial tissue fibrosis identified by delayed enhancement MRI and atrial fibrillation catheter ablation: the DECAAF study. *JAMA* 2014;**311**:498–506.
4. den Uijl DW, Delgado V, Bertini M, Tops LF, Trines SA, van de Veire NR, Zeppenfeld K, Schalij MJ, Bax JJ. Impact of left atrial fibrosis and left atrial size on the outcome of catheter ablation for atrial fibrillation. *Heart* 2011;**97**:1847–1851.
5. Burstein B, Nattel S. Atrial fibrosis: mechanisms and clinical relevance in atrial fibrillation. *J Am Coll Cardiol* 2008;**51**:802–809.
6. Nattel S, Burstein B, Dobrev D. Atrial remodeling and atrial fibrillation: mechanisms and implications. *Circ Arrhythm Electrophysiol* 2008;**1**:62–73.
7. Siebermair J, Kholmovski EG, Marrouche N. Assessment of left atrial fibrosis by late gadolinium enhancement magnetic resonance imaging: methodology and clinical implications. *JACC Clin Electrophysiol* 2017;**3**:791–802.
8. McGann C, Akoum N, Patel A, Kholmovski E, Revelo P, Damal K, Wilson B, Cates J, Harrison A, Ranjan R, Burgon NS, Greene T, Kim D, Dibella EV, Parker D, Macleod RS, Marrouche NF. Atrial fibrillation ablation outcome is predicted by left atrial remodeling on MRI. *Circ Arrhythm Electrophysiol* 2014;**7**:23–30.
9. Parmar BR, Jarrett TR, Kholmovski EG, Hu N, Parker D, MacLeod RS, Marrouche NF, Ranjan R. Poor scar formation after ablation is associated with atrial fibrillation recurrence. *J Interv Card Electrophysiol* 2015;**44**:247–256.
10. Boyle PM, Zahid S, Trayanova NA. Using personalized computer models to customtailor ablation procedures for atrial fibrillation patients: are we there yet? *Expert Rev Cardiovasc Ther* 2017;**15**:339–341.
11. Boyle PM, Hakim JB, Zahid S, Franceschi WH, Murphy MJ, Vigmond EJ, Dubois R, Haissaguerre M, Hocini M, Jais P, Trayanova NA, Cochet H. Comparing reentrant drivers predicted by image-based computational modeling and mapped by electrocardiographic imaging in persistent atrial fibrillation. *Front Physiol* 2018;**9**:414.
12. Roy A, Varela M, Aslanidi O. Image-based computational evaluation of the effects of atrial wall thickness and fibrosis on re-entrant drivers for atrial fibrillation. *Front Physiol* 2018;**9**:1352.
13. Zahid S, Cochet H, Boyle PM, Schwarz EL, Whyte KN, Vigmond EJ, Dubois R, Hocini M, Haissaguerre M, Jais P, Trayanova NA. Patient-derived models link re-entrant driver localization in atrial fibrillation to fibrosis spatial pattern. *Cardiovasc Res* 2016;**110**:443–454.
14. Zahid S, Whyte KN, Schwarz EL, Blake RC 3rd, Boyle PM, Chrispin J, Prakosa A, Ipek EG, Pashakhanloo F, Halperin HR, Calkins H, Berger RD, Nazarian S, Trayanova NA. Feasibility of using patient-specific models and the "minimum cut" algorithm to predict optimal ablation targets for left atrial flutter. *Heart Rhythm* 2016;**13**:1687–1698.
15. McDowell KS, Zahid S, Vadakkumpadan F, Blauer J, MacLeod RS, Trayanova NA. Virtual electrophysiological study of atrial fibrillation in fibrotic remodeling. *PLoS One* 2015;**10**:e0117110.
16. McDowell KS, Vadakkumpadan F, Blake R, Blauer J, Plank G, MacLeod RS, Trayanova NA. Methodology for patient-specific modeling of atrial fibrosis as a substrate for atrial fibrillation. *J Electrocardiol* 2012;**45**:640–645.
17. Roney CH, Bayer JD, Zahid S, Meo M, Boyle PM, Trayanova NA, Haissaguerre M, Dubois R, Cochet H, Vigmond EJ. Modelling methodology of atrial fibrosis affects rotor dynamics and electrograms. *Europace* 2016;**18**:iv146–iv155.
18. Cochet H, Dubois R, Yamashita S, Al Jefairi N, Berte B, Sellal JM, Hooks D, Frontera A, Amraoui S, Zemoura A, Denis A, Derval N, Sacher F, Corneloup O, Latrabe V, Clement-Guinaudeau S, Relan J, Zahid S, Boyle PM, Trayanova NA, Bernus O, Montaudon M, Laurent F, Hocini M, Haissaguerre M, Jais P. Relationship between fibrosis detected on late gadolinium-enhanced cardiac magnetic resonance and re-entrant activity assessed with electrocardiographic imaging in human persistent atrial fibrillation. *JACC Clin Electrophysiol* 2018;**4**:17–29.
19. Boyle PM, Hakim JB, Zahid S, Franceschi WH, Murphy MJ, Prakosa A, Aronis KN, Zghaib T, Balouch M, Ipek EG, Chrispin J, Berger RD, Ashikaga H, Marine JE, Calkins H, Nazarian S, Spragg DD, Trayanova NA. The fibrotic substrate in persistent atrial fibrillation patients: comparison between predictions from computational modeling and measurements from focal impulse and rotor mapping. *Frontiers in Physiology* 2018;**9**:1151.

20. McDowell KS, Vadakkumpadan F, Blake R, Blauer J, Plank G, Macleod RS, Trayanova NA. Mechanistic inquiry into the role of tissue remodeling in fibrotic lesions in human atrial fibrillation. *Biophys J* 2013;**104**:2764–2773.
21. Boyle PM, Zahid S, Trayanova NA. Towards personalized computational modelling of the fibrotic substrate for atrial arrhythmia. *Europace* 2016;**18**:iv136–iv145.
22. Yushkevich PA, Piven J, Hazlett HC, Smith RG, Ho S, Gee JC, Gerig G. User-guided 3D active contour segmentation of anatomical structures: significantly improved efficiency and reliability. *Neuroimage* 2006;**31**:1116–1128.
23. Akoum N, Daccarett M, McGann C, Segerson N, Vergara G, Kuppahally S, Badger T, Burgon N, Haslam T, Kholmovski E, Macleod R, Marrouche N. Atrial fibrosis helps select the appropriate patient and strategy in catheter ablation of atrial fibrillation: a DE-MRI guided approach. *J Cardiovasc Electrophysiol* 2011;**22**:16–22.
24. Khurram IM, Beinart R, Zipunnikov V, Dewire J, Yarmohammadi H, Sasaki T, Spragg DD, Marine JE, Berger RD, Halperin HR, Calkins H, Zimmerman SL, Nazarian S. Magnetic resonance image intensity ratio, a normalized measure to enable interpatient comparability of left atrial fibrosis. *Heart Rhythm* 2014;**11**:85–92.
25. Prassl AJ, Kickinger F, Ahammer H, Grau V, Schneider JE, Hofer E, Vigmond EJ, Trayanova NA, Plank G. Automatically generated, anatomically accurate meshes for cardiac electrophysiology problems. *IEEE Trans Biomed Eng* 2009;**56**:1318–1330.
26. Zghaib T, Ipek EG, Zahid S, Balouch MA, Misra S, Ashikaga H, Berger RD, Marine JE, Spragg DD, Zimmerman SL, Zipunnikov V, Trayanova N, Calkins H, Nazarian S. Association of left atrial epicardial adipose tissue with electrogram bipolar voltage and fractionation: electrophysiologic substrates for atrial fibrillation. *Heart Rhythm* 2016;**13**:2333–2339.
27. Courtemanche M, Ramirez RJ, Nattel S. Ionic mechanisms underlying human atrial action potential properties: insights from a mathematical model. *Am J Physiol* 1998;**275**:H301–H321.
28. Krummen DE, Bayer JD, Ho J, Ho G, Smetak MR, Clopton P, Trayanova NA, Narayan SM. Mechanisms of human atrial fibrillation initiation: clinical and computational studies of repolarization restitution and activation latency. *Circ Arrhythm Electrophysiol* 2012;**5**:1149–1159.
29. Deng D, Murphy MJ, Hakim JB, Franceschi WH, Zahid S, Pashakhanloo F, Trayanova NA, Boyle PM. Sensitivity of reentrant driver localization to electrophysiological parameter variability in image-based computational models of persistent atrial fibrillation sustained by a fibrotic substrate. *Chaos* 2017;**27**:093932.
30. Hakim JB, Murphy MJ, Trayanova NA, Boyle PM. Arrhythmia dynamics in computational models of the atria following virtual ablation of re-entrant drivers. *Europace* 2018;**20**:iii45–iii54.
31. Ramos-Mondragon R, Galindo CA, Avila G. Role of TGF-beta on cardiac structural and electrical remodeling. *Vasc Health Risk Manag* 2008;**4**:1289–1300.
32. Vigmond EJ, Weber dos Santos R, Prassl AJ, Deo M, Plank G. Solvers for the cardiac bidomain equations. *Prog Biophys Mol Biol* 2008;**96**:3–18.
33. Plank G, Zhou L, Greenstein JL, Cortassa S, Winslow RL, O'Rourke B, Trayanova NA. From mitochondrial ion channels to arrhythmias in the heart: computational techniques to bridge the spatio-temporal scales. *Philos Trans A Math Phys Eng Sci* 2008;**366**:3381–3409.
34. Cochet H, Mouries A, Nivet H, Sacher F, Derval N, Denis A, Merle M, Relan J, Hocini M, Haissaguerre M, Laurent F, Montaudon M, Jais P. Age, atrial fibrillation, and structural heart disease are the main determinants of left atrial fibrosis detected by delayed-enhanced magnetic resonance imaging in a general cardiology population. *J Cardiovasc Electrophysiol* 2015;**26**:484–492.
35. Jalife J, Kaur K. Atrial remodeling, fibrosis, and atrial fibrillation. *Trends Cardiovasc Med* 2015;**25**:475–484.
36. Boldt A, Wetzel U, Lauschke J, Weigl J, Gummert J, Hindricks G, Kottkamp H, Dhein S. Fibrosis in left atrial tissue of patients with atrial fibrillation with and without underlying mitral valve disease. *Heart* 2004;**90**:400–405.
37. Kostin S, Klein G, Szalay Z, Hein S, Bauer EP, Schaper J. Structural correlate of atrial fibrillation in human patients. *Cardiovasc Res* 2002;**54**:361–379.
38. Kottkamp H, Berg J, Bender R, Rieger A, Schreiber D. Box isolation of fibrotic areas (BIFA): a patient-tailored substrate modification approach for ablation of atrial fibrillation. *J Cardiovasc Electrophysiol* 2016;**27**:22–30.
39. Narayan SM, Krummen DE, Rappel WJ. Clinical mapping approach to diagnose electrical rotors and focal impulse sources for human atrial fibrillation. *J Cardiovasc Electrophysiol* 2012;**23**:447–454.
40. Haissaguerre M, Hocini M, Denis A, Shah AJ, Komatsu Y, Yamashita S, Daly M, Amraoui S, Zellerhoff S, Picat MQ, Quotb A, Jesel L, Lim H, Ploux S, Bordachar P, Attuel G, Meillet V, Ritter P, Derval N, Sacher F, Bernus O, Cochet H, Jais P, Dubois R. Driver domains in persistent atrial fibrillation. *Circulation* 2014;**130**:530–538.
41. Verheule S, Sato T, Everett T, Engle SK, Otten D, Rubart-von der Lohe M, Nakajima HO, Nakajima H, Field LJ, Olgin JE. Increased vulnerability to atrial fibrillation in transgenic mice with selective atrial fibrosis caused by overexpression of TGF-beta1. *Circ Res* 2004;**94**:1458–1465.
42. Tanaka K, Zlochiver S, Vikstrom KL, Yamazaki M, Moreno J, Klos M, Zaitsev AV, Vaidyanathan R, Auerbach DS, Landas S, Guiraudon G, Jalife J, Berenfeld O, Kalifa J. Spatial distribution of fibrosis governs fibrillation wave dynamics in the posterior left atrium during heart failure. *Circ Res* 2007;**101**:839–847.
43. Hansen BJ, Zhao J, Csepe TA, Moore BT, Li N, Jayne LA, Kalyanasundaram A, Lim P, Bratasz A, Powell KA, Simonetti OP, Higgins RS, Kilic A, Mohler PJ, Janssen PM, Weiss R, Hummel JD, Fedorov VV. Atrial fibrillation driven by micro-anatomic intramural re-entry revealed by simultaneous sub-epicardial and sub-endocardial optical mapping in explanted human hearts. *Eur Heart J* 2015;**36**:2390–2401.
44. Zhao J, Hansen BJ, Wang Y, Csepe TA, Sul LV, Tang A, Yuan Y, Li N, Bratasz A, Powell KA, Kilic A, Mohler PJ, Janssen PML, Weiss R, Simonetti OP, Hummel JD, Fedorov VV. Three-dimensional integrated functional, structural, and computational mapping to define the structural "fingerprints" of heart-specific atrial fibrillation drivers in human heart *ex vivo*. *J Am Heart Assoc* 2017;**6**:2390–2401.
45. Morgan R, Colman MA, Chubb H, Seemann G, Aslanidi OV. Slow conduction in the border zones of patchy fibrosis stabilizes the drivers for atrial fibrillation: insights from multi-scale human atrial modeling. *Front Physiol* 2016;**7**:474.
46. Lalani GG, Coysh T, Baykaner T, Zaman J, Hopper K, Schricker AA, Trikha R, Clopton P, Krummen DE, Narayan SM. Organized sources are spatially conserved in recurrent compared to pre-ablation atrial fibrillation: further evidence for non-random electrical substrates. *J Cardiovasc Electrophysiol* 2016;**27**:661–669.
47. Tao S, Guttman MA, Fink S, Elahi H, Patil KD, Ashikaga H, Kolandaivelu AD, Berger RD, Halushka MK, Schmidt EJ, Herzka DA, Halperin HR. Ablation lesion characterization in scarred substrate assessed using cardiac magnetic resonance. *JACC Clin Electrophysiol* 2018;**5**:91–100.
48. Lin T, Rillig A, Bucur T, Metzner A, Mathew S, Wissner E, Wohlmuth P, Kuck KH, Ouyang F, Tilz RR. Focal impulse and rotor modulation using the novel 64-electrode basket catheter: electrogram characteristics of human rotors. *Europace* 2015;**17**:1791–1797.